Cumulative Component Damages on Collapse Capacity of Ductile Steel and CFT Moment Resisting Frames under Over-design Ground Motions

Y. Bai[a,b], X. Ma[c], B. Wang[d*] and G. Cao[d], Michael Beer[b,e,f]

[a] School of Civil Engineering, Chongqing University, Chongqing, 400044, China; [b] Institute for Risk and Reliability, Leibniz University of Hannover, 30167 Hannover, Germany; [c] China Railway First Survey and Design Institute Group Co., Ltd., Xian 710043, China; [d] School of Civil Engineering, Chang'an University, Xi'an, 710061, China; [e] The University of Liverpool, Institute for Risk and Uncertainty, Peach Street, L69 7ZF Liverpool, United Kingdom; [f] Tongji University, International Joint Research Center for Engineering Reliability and Stochastic Mechanics, Shanghai 200092, China

[*] Corresponding author: chnwangbo@chd.edu.cn; Tel.: +86-137-2045-3378

Abstract: Great earthquakes are likely to generate over-design ground motions leading to the dissatisfactory seismic demand and severe damages of structural components in general high-rise steel moment-resisting frames (SMRFs). Overall seismic behavior of high-rise SMRFs may be significantly affected by the local failure of members. This paper focuses on the margins of deterioration and collapse of 40-story SMRFs and the equivalent MRFs with concrete-filled tubular (CFT) columns considering the strength deterioration effect in constitutive models designed by current building standards. The input long-period ground motions are synthetic earthquake waves with flat velocity spectral shape. Deterioration and collapse criteria of models based on the peak ground motion velocity are estimated by performing the incremental dynamic analysis (IDA) The results indicate that the collapse mechanism was formed in the lower stories of high-rise SMRFs under the very rare earthquake. The strength and stiffness deterioration significantly amplified the damage extent and the influence degree depends on the sectional compactness of components. And the MRF with concrete-filled tubular (CFT) columns has a higher collapse margin against overall collapse compared with SMRFs.

Keywords: Seismic damage; Member deterioration; Collapse prevention; Cumulative plastic deformation ratio; High-rise buildings

1 Introduction

In recent decades, extreme earthquakes brought severe damages to buildings and infrastructures [Architectural Institute of Japan, 2011]. During the Tokachi earthquake, excessive seismic responses of oil tanks were attacked by long-period ground motions associated with long-duration have been concerned. This phenomenon leads to a new understanding of the seismic performance indicator of the structures with a large range of natural periods. For instance, the seismic collapse capacity of tall buildings might be dominated by the accumulation of member damages rather than maximum drift responses. Hence, new sensing techniques of damage identification and modeling method for quantitatively evaluating the extent of local damages are necessitated by the resonance under the over-design earthquake.

The high-rise buildings with first mode period ranging from 3 sec to 6 sec are vulnerable to sustain damages by the ground motions occurred nearby. Thus, the earthquake-induced component damages and energy-dissipating capacity in building structures become important for assessing the overall collapse safety of buildings [Lin *et al*., 2018]. Energy dissipation has been treated as an indicator of the seismic performance of building structures since Housner [1956] initially proposed an energy-based approach for seismic design of structures. Akiyama et al. [1985] proposed the relation between the energy-dissipating capacity of the structure and its corresponding demand by using an indicator of cumulative plastic deformation. It is well known that Park and Ang [1985] proposed a damage index based on maximum plastic deformation and hysteretic energy. Thereafter, Khashaee [2005] proposed a new damage index based on ductility and stiffness deterioration for seismic design of structures, whereas the strength deterioration due to the local failures of structural components has been neglected. Recently, several researchers proposed damage and energy concepts for seismic analysis and design of moment frames [Fajfar and Gasperisic, 1996; Mehanny and Deierlein, 2001; Khashaee, 2005; Bojórquez *et al*., 2010; Karavasilis *et al*., 2012; Wong and Harris, 2012; Heidari and Gharehbaghi, 2015; Diaz *et al*., 2017; Ke *et al*., 2017]. Deniz *et al*. [2017] have been found that the energy-based criterion of structural components is more reliable for predicting the earthquake-induced collapse of frames. Those works suggested that energy-based damage indices could be used to quantitatively evaluate the seismic performance near the so-called “collapse criterion” of steel moment-resisting frames (SMRFs) and composite moment resisting frames with consideration of the high level of nonlinear behavior, i.e. member deterioration in strength and stiffness.

The fiber element method which considers the strength deterioration (SD) due to local buckling by defining the stress-strain relationship has been adopted as a simple numerical approach for evaluating the non-linear behavior of center-lined beam and column members as shown in Figure 1. The moment-rotation relation at beam and column ends in SMRFs can be integrated from the sectional stresses and strains of each fiber layer, and subsequently controls the collapse curve between earthquake intensity and performance indicator at the building level. Nonetheless, fiber element is characterized by certain inherent limitations such as plane assumption for cross-sections and the lack of capacity to emulate the buckling modes of thin-walled sections [Spacone and El-Tawil, 2004].

This paper quantitively dealt with the collapse margin of high-rise SMRFs and equivalent MRF model with concrete infilled steel tubular (CFT) columns (CFT-MRFs) by gradually increasing the intensity of synthetic ground motion waves with flat velocity spectral shape. The peak ground velocity (PGV) was selected as the index of deterioration and collapse criteria of high-rise buildings since the maximum response of high-rise buildings under over-design earthquakes occurred nearby mainly depends on PGV which significantly influences the total input energy. Simplified stress-strain relationships for steel were defined to account for the SD effect occurred in steel tubes since the stiffness and strength deterioration of steel members under cyclic loading plays a significant influence on the failure mechanism. Then 40-story SMRF and CFT-MRF models based on fiber discretized layers that incorporate the component SD effects with various deteriorating levels were built. Finally, the overall collapse mechanisms of these models under over-design earthquakes were identified based on the local damage caused by the SD effect.

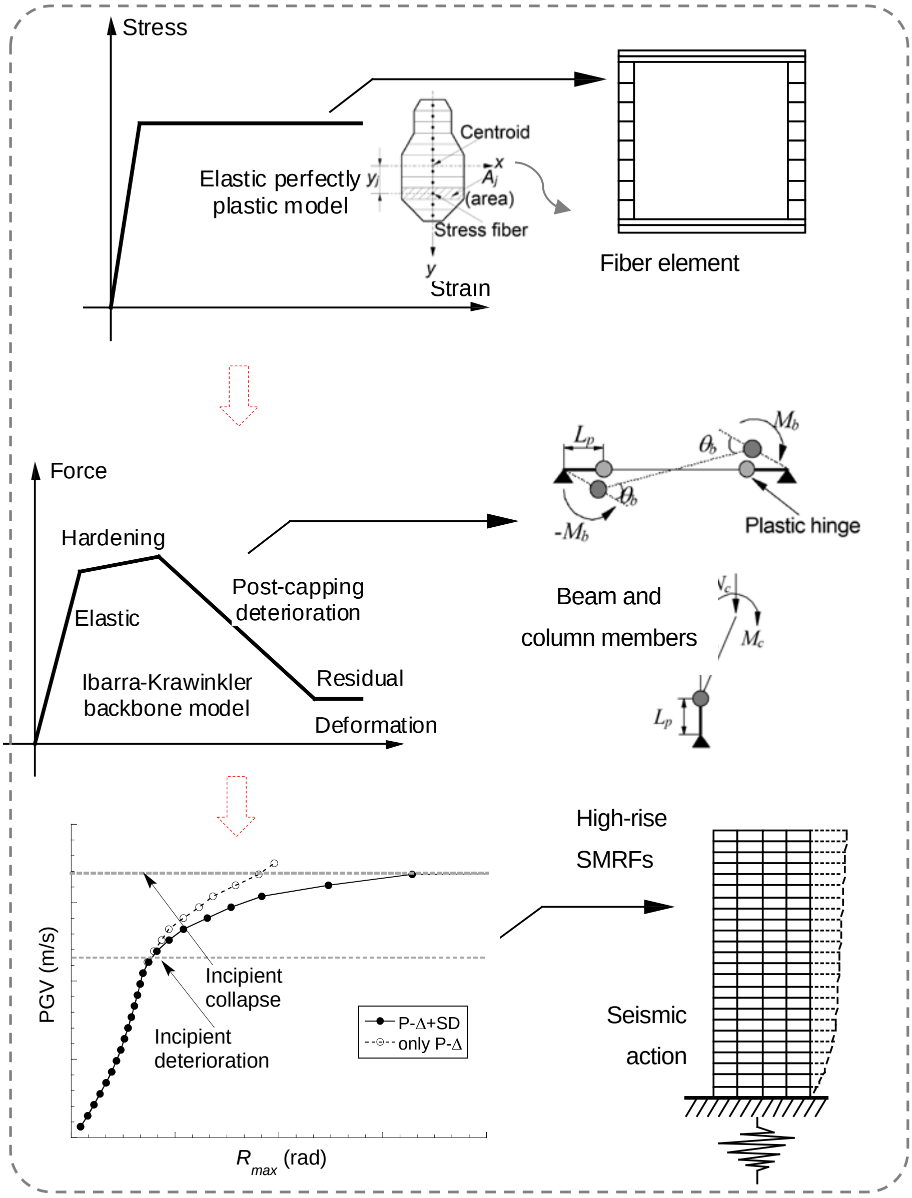

Fig. 1 The process of seismic collapse analysis using fiber element model

2 High-rise benchmarks and seismic excitations

2.1 Constitutive models of fiber elements

The constitutive model for rectangular steel tube and H-shaped steel elements considering strength deterioration caused by local buckling, Bauschinger effect, and unloading stiffness deterioration, as shown in Figure 2, is developed based on the Menegotto-Pinto model [1973], to be capable of capturing the effect of member deterioration on the seismic damages and collapse-resistant capacity of high-rise SMRFs and CFT-MRFs. Strength deterioration (SD) after local buckling of steel beams or columns can be accounted for a negative slope in the compression side of the stress-strain relationship for steel elements. As shown in Figure 2, σ_{lb} and ε_{lb} is the critical stress and strain corresponding to local buckling, respectively; γ_{lb} is the residual stress after strength deterioration; τ_{lb} and τ_{re} are the ratio of negative modulus and residual modulus to Young's modulus (E), respectively. In this stress-strain model, the influence of local buckling-induced damages on the compressive strength (σ_{lb}) and strain softening (τ_{lb} and τ_{re}) have been taken into account.

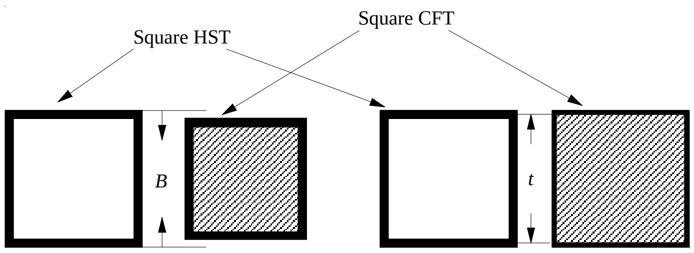

Fig. 2 Equivalent square CFT and HST column

Figure 3 presents the Sakino-Sun model, which considers the confining effect of the in-filled concrete in square CFT columns on the concrete compressive strength and deformation ability. As shown in Figure 3, the flat curve after peak-point is analogous to the non-deterioration situation, while the post-peak deterioration is considered by capturing the inflection point of the Sakino-Sun model to maintain equilibrium in deterioration and residual branches. To respectively predict the deterioration gradient and residual strength of the confined concrete, we specifically simplified the deterioration branch (post-peak branch and residual branch) as a bilinear relation, where the transit point (X_{cu}, Y_{cu}) between the post-peak branch and the residual branch is defined by

$$\begin{cases} X_{cu} = \dfrac{\varepsilon'_{cu}}{\varepsilon'_{cc}} = 1.96\left(\dfrac{V}{W}\right)^{0.88} + 4.77 \\ Y_{cu} = \dfrac{\sigma'_{cu}}{f'_{cc}} = \lim\limits_{X\to\infty} \dfrac{VX + (W-1)X^2}{1+(V-2)X+WX^2} = 1 - \dfrac{1}{W} \end{cases} \tag{1}$$

$$V = E_c \times \frac{f'_{cc}}{\varepsilon'_{cc}} \tag{2}$$

$$W = 1.50 - 17.1\times10^{-3} f'_c + 2.39\times\sigma_{re}^{0.5} \tag{3}$$

$$X = \frac{\varepsilon_c}{\varepsilon_{cc}^{'}} \tag{4}$$

where $f_{cc}^{'}$ is the compressive strength and compressive strain of the confined concrete, respectively; $f_c^{'}$ and $\varepsilon_c^{'}$ are the compressive stress and strain, respectively; E_c is the elastic modulus of the plain concrete; $\sigma_{re}^{0.5}$ is the radial force confining stress; $\sigma_{cu}^{'}$ and $\varepsilon_{cu}^{'}$ are the compressive stress and strain at the transit point, respectively.

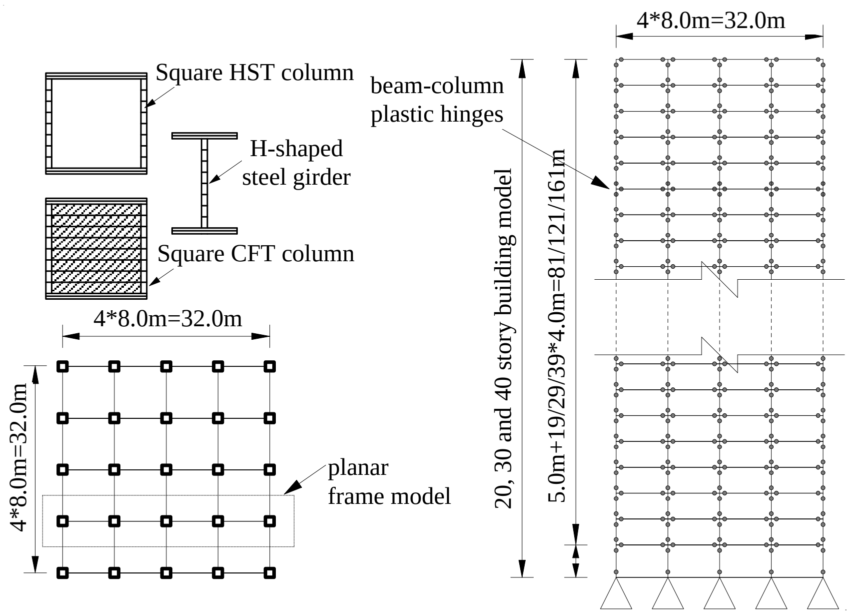

Fig. 3 Component section, plane and elevation views of high-rise building models

Hence, stress-strain models considering the strength and stiffness deterioration for steel members, including H-shaped steel beams, square hollow steel tubular (HST) and CFT columns, and the confined concrete in square CFT members have been built, based on an extensive database of such structural members. Thereafter, as shown in Figure 1, the fiber section of beam ends and column bases follows the above constitutive model for simulating the nonlinear responses, while the middle parts of beams and columns remain elastic.

2.2 Compactness ranks of HST columns and CFT columns

Sectional compactness of H-shaped steel beam and square HST columns can be generally specified by the geometric width-to-thickness ratio of cross-sections, such as B/t_f and D/t_w for flange and web of beams, respectively, and B/t for columns. Table 1 characterizes the FA and FB levels, which are respectively equivalent to the compact and non-compact sectional properties. As shown in Table1, the differences in the critical width-to-thickness ratio of the column, beam flange and beam web with FA and FB levels utilizing SM490 steels are respectively 12.12%, 22.22%, and 8.33%. Table 2 shows the characteristic points about strength deterioration in deteriorating constitutive of FA and FB levels. As shown in Table 2, the ratio of stiffness compared to Young's modulus (η_{b}) in the post-peak deterioration phase of FA column demonstrates a smaller value than that of FB column, which suggests that the compact column shows smaller strength deterioration than the non-compact column after local buckling. Also, the critical strain at local buckling of FB ranked column section ($\varepsilon_{lb,\ FB}$>0.64%) is smaller than that of FA column section ($\varepsilon_{lb,\ FA}$>0.86%), indicating that the FB column is vulnerable to sustain local buckling induced damages resulting in significant deterioration of stiffness and strength. For the mild steel SM490, the nominal yield strength (σ_y) is 325 MPa, the ultimate strength (σ_u) is 490 MPa, and Young's modulus E_s is 2.05$\times$ 10^5MPa.

Based on the various statistical databases [Architectural Institute of Japan, 2007], SMRF was the dominant structural system in Japan from 1980 s to 90 s, and the overall heights mainly ranged from 80 to 160 m. At present, CFT-MRFs which have been increasing in the engineering practices of high-rise buildings hardly experienced a great earthquake and limited numerical study was addressed on collapse simulation of high-rise SMRFs with CFT columns. Therefore, the assessment of their seismic safety under severe seismic excitations is necessary. Furthermore, to compare and quantify the collapse margin of high-rise CFT buildings to analogical high-rise steel buildings, only the square HST columns in high-rise SMRF models are replaced by the square CFT columns based on equivalent horizontal stiffness K [(12EI)/l3]. Figure 4 is the two equivalent methods from the HST column to the CFT column. As shown in Figure 4, the equivalent square CFT column can make the tubular column section more compact by reducing the side length, compared with the square HST column, or save the steel material by reducing the thickness of the steel tube. Both of the above advantages show different damage propagation in strength and stiffness for the CFT column, one is material dominated, the other is geometric property dominated.

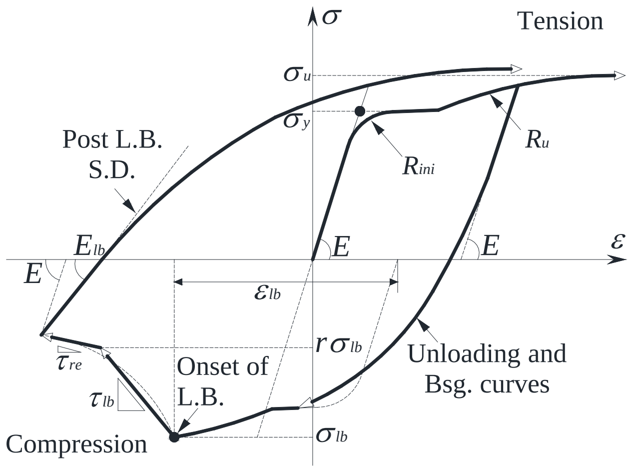

Fig. 4 Damage stress-strain model for steel elements

2.3 High-rise SMRF and CFT-MRF models

To be analogous to FA_c-FA_b and FB_c-FB_b SMRF models, where FA_c and FA_b represent the column and beam with compact section, respectively, and FB_c and FB_b represent the column and beam with non-compact section, respectively, we adopt the CFT columns with the compact and non-compact section in CFT-MRF models, i.e. CFT-MRF model with FA_c-FA_b and CFT-MRF model with FB_c-FB_b. Here the compact squared CFT columns are specified by the width-to-thickness ratio and axial load ratio, for instance, the compact column with the maximum axial load ratio 0.3 corresponds to the *B/t* of 37[Bai *et al*., 2017].

Since the overall height affects the global stiffness, second-order (P-Δ) effect and axial forces at lower stories, and preliminary numerical analysis indicated that the member deterioration in lower stories of 40-story steel building model caused by P-Δ effect was more evident compared with 20-story model and 30-story model, planar moment frame models of 40-story S/CFT-MRF considering various deteriorating levels utilizing SM490 are seismic designed by current building standards to evaluate the influence of the SD effect on the damage and collapse behavior. And Column over-strength factor met the demand between 1.5 and 2.0, and consistent steel and concrete materials were adopted in various building models. Meet the so-called strong-column weak-beam concept to prevent undesirable collapse. All the models meet the so-called strong-column weak-beam concept to prevent undesirable collapse. Figure 5 illustrates the component section, elevation, and plan views of planar models. It can be observed that the story height was set to be 4.0 m for the standard story and 5.0 m for the bottom story, and 8.0 m for column distance. Therefore, a total of two SMRFs (labeled as the 40S-FA_c-FA_b model and 40S-FB_c-FB_b model), and two CFT-MRFs numerical models (labeled as the 40CFT-FA_c-FA_b model and 40CFT-FB_c-FB_b model) were built. The cross-sectional properties of the 40-story steel models are shown in Table 3and Table 4. And the natural periods of models are listed in Table 5.

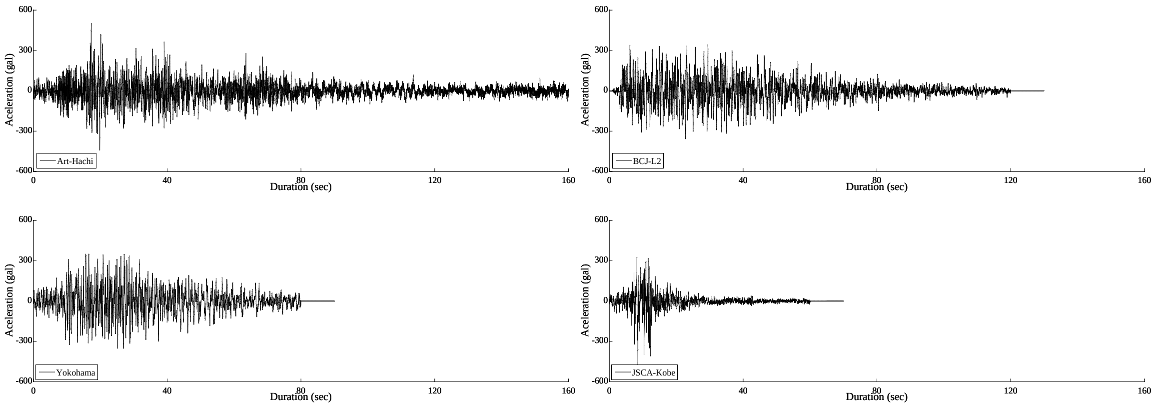

Fig. 5 Time history acceleration of flat-shaped ground motions

2.4 Synthetic earthquake waves

To simulate large earthquake excitations on high-rise buildings and also try to relatively eliminate the record-to-record uncertainty, synthetic ground motions (i.e. Art-Hachi, BCJ-L2, Yokohama, and JSCA-Kobe) characterized with the flat shape of velocity spectra are chosen for incremental dynamic analysis (IDA). Figure 6 presents the acceleration time history curves of those input waves. It can be seen that the durations of Art-Hachi, BCJ-L2, JSCA-Kobe, and Yokohama moves are approximately 163.8 sec, 120.0 sec, 60.0 sec, and 80.0 sec, respectively, and their corresponding original PGVs are 64.0 kine, 80.4 kine, 58.7 kine, and 62.0 kine respectively. The maximum and cumulative member damages of various high-rise MRFs subjected to over-design ground motions are assessed based on IDA controlled by the incremental factor φ from elastic to collapse, based on the PGV of each artificial wave.

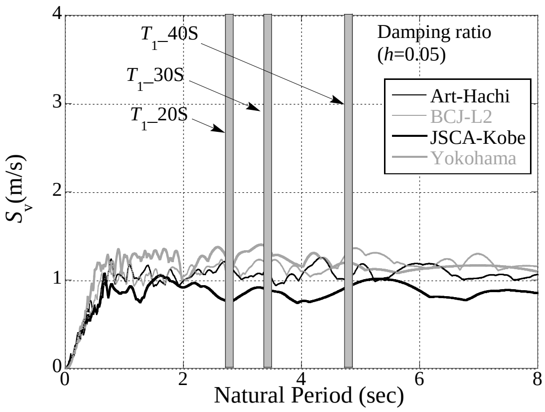

Fig. 6 Pseudo velocity response spectrum of artificial earthquake waves

Additionally, Figure 7 shows the pseudo velocity spectral responses of these synthetic waves, it can be observed that nearly flat maximum velocity responses are observed in the range of long 'first-mode' natural periods of high-rises models.

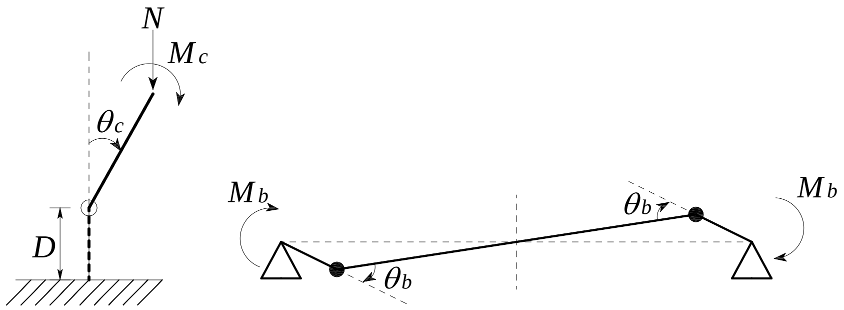

(a) Column bases (b) beam ends

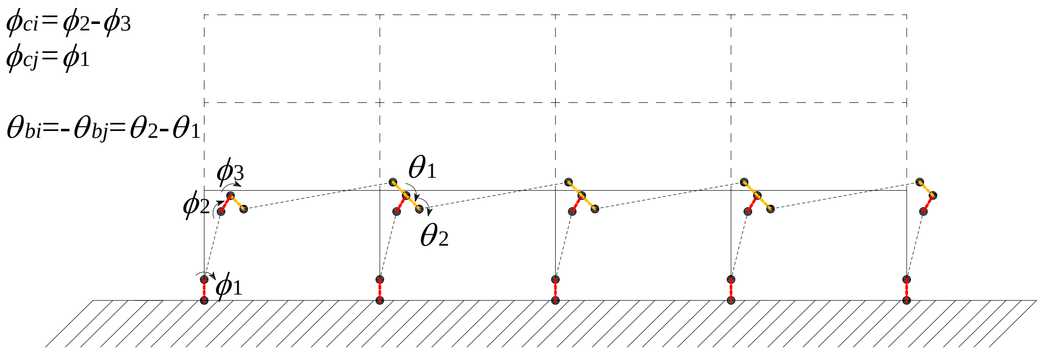

(c) Rotational relation of beam and column components

Fig. 7 Plastic deformation mechanism of steel moment frames

3 Simulation Results and Discussion

3.1 Plastic deformation ratio

Plastic deformation is used for quantifying the extent of the plastic-deformation capacity of local regions [Wakabayashi, 1986]. Local buckling and damage of steel members can be evaluated by normalized rotation of steel members, i.e., ductility ratio. The strength and stiffness deteriorating of various steel and CFT members caused by local buckling show significant influence on the nonlinear dynamic's responses [Bai *et al*, 2012]. Thus, more plastic hinges and larger ductility ratios are correspondingly induced at the beam ends and column bases in high-rise MRF buildings designed with weak-beam strong-column.

The effect of member deterioration on the local-responses (i.e. component responses) of the critical regions (i.e., plastic hinges) in existing high-rise SMRFs is focused, to reveal how much the member damages of such structures has been initiated. For high-rise structures under time-history earthquake excitations, maximum ductility ratios of H-shaped steel beam and square HST/CFT column bases at the bottom story (μ_b and μ_c) are feasible to be treated as the damage index, which is calculated by

$$\begin{cases} \text{Max.}\mu_{\text{b}} = \dfrac{\max(\theta_{\text{b}})}{\theta_{\text{y}}} \\ \text{Max.}\mu_{\text{c}} = \dfrac{\max(\theta_{\text{c}})}{\theta_{\text{y}}} \end{cases} \tag{2}$$

where max(θ_b) and max(θ_c) are the maximum rotations of the plastic hinge at beam ends and column bases, respectively; θ_y is the rotation at yield point of the beam or column members that is calculated by $\theta_y = M_y/K$; K is the flexural stiffness of beam/column members that is calculated by K=6EI/l; M_y is the bending moment capacity at yield point that is calculated by $M_y=Z\times F_y$; Z is section modulus that is calculated by $Z = I/(D/2)$; F_y is yielding strength of steel materials.

Figure 8 shows the rotation of the plastic hinge at column bases, beam end, and the rotational relationship of beam and column components. Figure 9 illustrates the plastic hinge mechanism of high-rise SMRF buildings with the weak-beam strong-column mechanism under the design-level earthquakes. As shown in Figure 9, the red line represents the residual deformation at the end, and the black lines represent the timely deformation responses. It is noted that plastic hinges at the column base in the bottom story of high-rise SMRF buildings could modify the side-sway of high-rise buildings and the phenomenon of deformation concentration can be observed at lower-story [Uetani, 1996]. Therefore, we respectively compare the plastic deformation ratios of beam ends and column bases between deteriorating and non-deteriorating models.

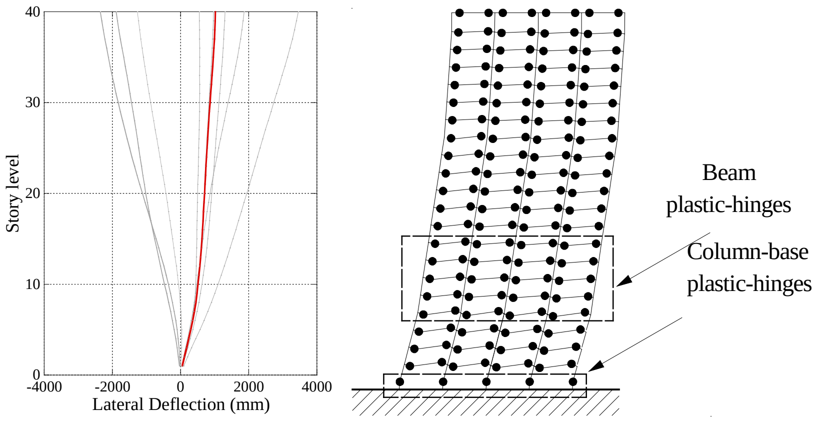

Fig. 8 Plastic-hinge mechanism of high-rise steel building

3.2 Deterioration margin and collapse margin based on earthquake intensity

Since the composite effects of the in-filled concrete and the hollow steel sectional column have been neglected in the design procedures of many high-rise steel structure buildings, it is necessary to explain properly how much does CFT-MRF building improve in resisting member deterioration compared with SMRF building when these buildings have close ultimate strength.

To evaluate the effect of member deterioration on the ductility ratios of high-rise buildings, the maximum ductility ratios of beam end and column bases in deteriorating and non-deteriorating SMRF and CFT-MRF models under IDA are analyzed (e.g., Art-Hachi).

Studies indicate that the total input energy of earthquakes has a high correlation with the spectrum characteristics of earthquakes, duration of earthquakes, and the PGV, and the intensity index represented by PGV has a high correlation with the structural seismic responses of high-rise buildings with a medium-long natural period. Although the correlation degree in the region of the short natural period and long period is slighter lower than that in the middle period range, the correlation is still ideal compared with another intensity index. Consequently, PGV is an appropriate seismic intensity index based on performance design and evaluation.

Also, AIJ adopts PGV as the evaluation index of intensity grade of ground motion. That is level

1 ground motion corresponds to a ground motion with a PGV of 0.25 m/s and level 1 ground motion corresponds to a ground motion with a PGV of 0. 5 m/s. Therefore, indexes for indicating the deterioration margin and collapse margin of high-rise SMRFs and CFT-MRFs concerning the intensity measure of level 2 (PGV=0.50 m/s) are separately proposed as follows

$$\begin{cases} \lambda_{\text{det}} = \dfrac{\text{PGV}_{\text{det}}}{\text{PGV}_{\text{level2}}} \\ \lambda_{\text{col}} = \dfrac{\text{PGV}_{\text{col}}}{\text{PGV}_{\text{level2}}} \end{cases} \tag{3}$$

where PGV_{det} and PGV_{col} are the PGVs correspondings to the deterioration and collapse of building, respectively.

Figures 10 and 11 presented the relationship between the maximum ductility ratios of members in the 40S-FA$_c$-FA$_b$ model and the 40CFT-FA$_c$-FA$_b$ model and the input peak ground velocity, respectively. It can be seen that the effect of member deterioration gradually shows the extensive influence on the maximum ductility ratios of beam ends and column bases.

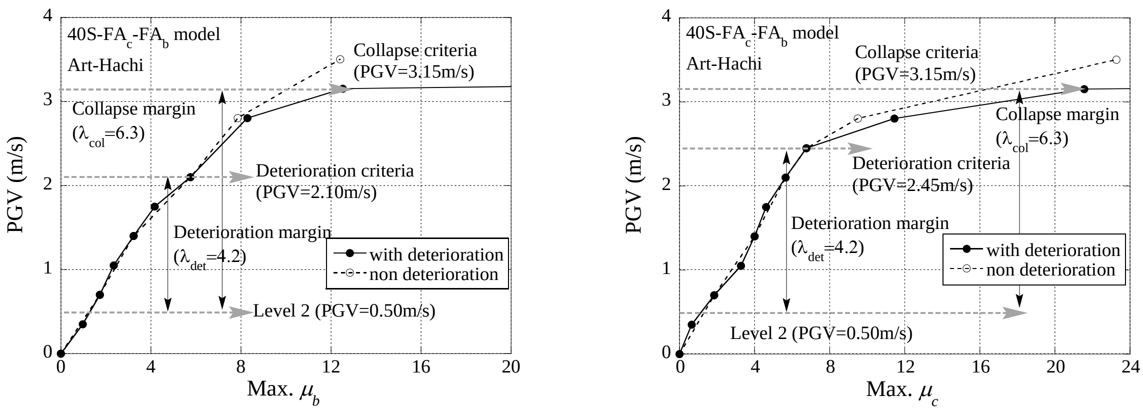

(a) Beam responses (b) Column responses

Fig. 9 Incremental responses of plastic deformation ratio in 40-story SMRF model

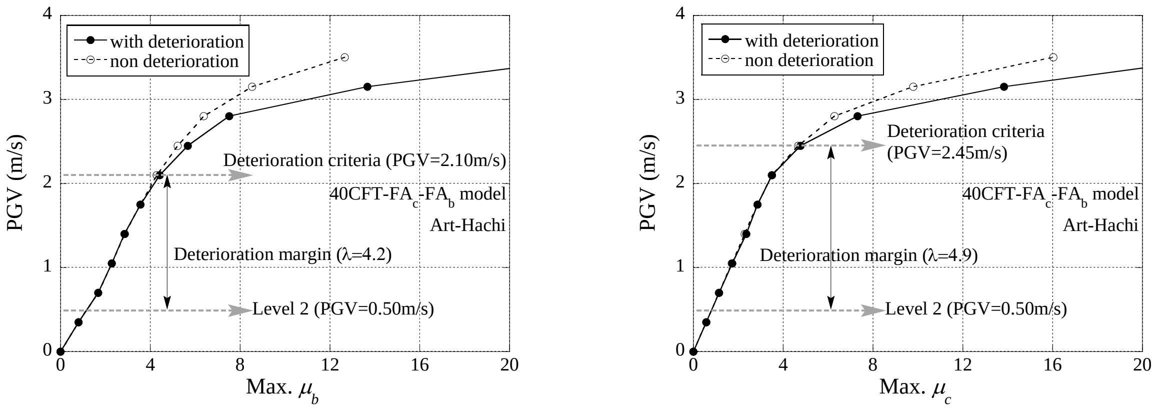

(a) Beam responses (b) Column responses

Fig. 10 Incremental responses of plastic deformation ratio in 40-story CFT-MRF model

As shown in Figures 10 (a) and 10 (b), the effect of member deterioration on ductility ratios of H-shaped steel beam and square HST column is initiated at the incremental factor φ equals to 3.0 and 3.5, respectively, which means that their deterioration margins are λ_{det}=4.2 and λ_{det}=4.9, respectively. Then after that, the seismic-resistant capacity of the 40S-FA$_c$-FA$_b$ model significantly deteriorates and collapse is induced eventually. Additionally, it is noted that the collapse of the beam and column is captured at the incremental factor of φ=4.5, indicating that the corresponding collapse margin is λ_{col}=6.3 for this low deterioration (Low-det.) high-rise SMRF buildings.

As shown in Figures 11(a) and 11 (b), the effect of member deterioration on ductility ratios of H-shaped steel beam and square CFT column is initially captured at the incremental factor of φ=3.0 and φ=3.5 respectively, the reason why column base deterioration emerges later than that of beam deterioration is that weak-beam mechanism makes beam firstly yield. However, the sway collapse of the 40CFT-FA$_c$-FA$_b$ model has not been observed at the end of the test, and the maximum PGV of beam and column components is 3.4m/s, indicating that λ_{col} is larger than 6.8, which is larger than that of the 40S-FA$_c$-FA$_b$ model.

Based on the viewpoint of seismic-redundancy of structures, deterioration margin, and collapse margin in terms of intensity measure (PGV) are assessed. Within the range of incremental factor φ ≤4.9, namely λ≤6.3, the collapse of the 40S-FA$_c$-FA$_b$ model is induced, while it is not feasible to 40CFT-FA$_c$-FA$_b$ model, indicating that high-rise CFT-MRFs had a higher safety margin since the local buckling of steel plate is delayed by the in-filled concrete, which enlarges the ductile behavior and stability of CFT columns compared to HST with equivalent stiffness.

Although the occurrence probability of ground motions with PGV equal to 200 kine and 300 kine is very low (corresponds to about 4 times and about 6 times the level 2 earthquake ground motion, respectively), there exists failure risks for existing structures. For instance, the maximum ground motions acquired in the Kobe Earthquake have the PGV of 90 kine, which is about twice the earthquake intensity of level 2 in Japan. Furthermore, during the Tohoku earthquake in 2011, the maximum ground motion captured by the MYG004 observatory, where the peak ground acceleration and velocity are respectively 2699 gal and 153 kine (3 times level 2). It is noted that the MYG004-NS wave can excite the spectral velocity reaching 483 kine at the natural period of 0.24-second structures. It means that the existing high-rise buildings or other infrastructures face essential damage and collapse risks when such a huge earthquake occurs in the soil foundation with resonant predominant periods.

3.3 Ductility ratios of local members in high-rise CFT-MRF models

To evaluate the effect of member deterioration on ductility ratios of local members in high-rise CFT-MRF buildings, the ductility ratio of the beam in the 40CFT-FA$_c$-FA$_b$ model and 40CFT-FB$_c$-FB$_b$ model are analyzed in Figures 12 (a) and 12 (b), respectively.

As shown in Figure 12, beams in both the 40CFT-FA$_c$-FA$_b$ model and the 40CFT-FB$_c$-FB$_b$ model are not affected by member deterioration at the early stage due to they were at elastic phases. Then after that the ductility ratios of the beam in the 40CFT-FA$_c$-FA$_b$ model gradually increased, while that in the 40CFT-FB$_c$-FB$_b$ model suddenly increased until failure, indicating the better mechanical performance of the 40CFT-FA$_c$-FA$_b$ model, compared to the 40CFT-FB$_c$-FB$_b$ model.

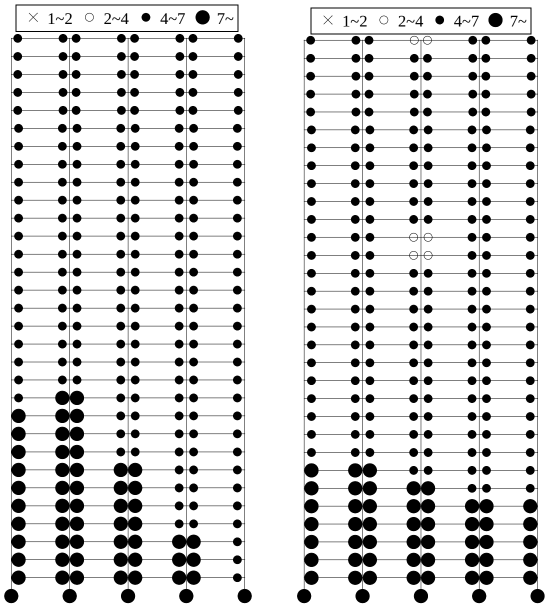

(a) Without deterioration (b) With deterioration

Fig. 11 Collapse of 40S-FA$_c$-FA$_b$

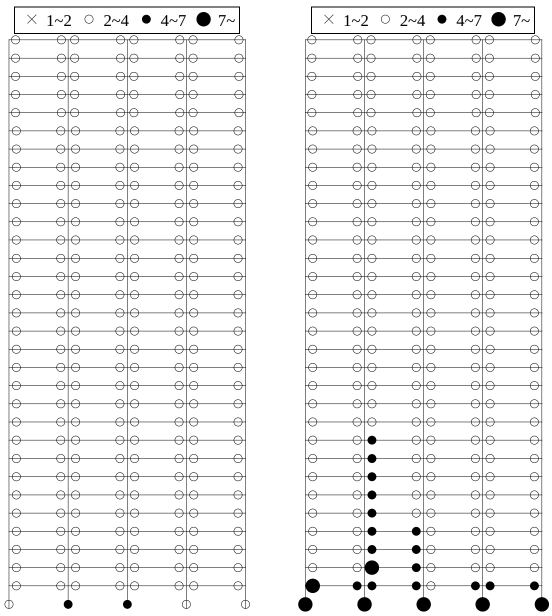

(a) Without deterioration (b) With deterioration

Fig. 12 Collapse of 40S-FB$_c$-FB$_b$

Besides, for the CFT frame designed by the weak-beam strong-column mechanism, the plastic hinge is easily induced at the column-base of the bottom story. Especially for the high-rise CFT building models subjected to incremental earthquake excitations, the plastic rotation at the CFT column-base of the bottom story significantly affects the side-sway pattern of the corresponding building. Thus, the ductility ratios of column bases of the 40CFT-FA$_c$-FA$_b$ model and 40CFT-FB$_c$-FB$_b$ model are also analogically analyzed as shown in Figure 13, respectively. It can be seen that the deterioration of the column in the 40CFT-FB$_c$-FB$_b$ model is much early than that in the 40CFT-FA$_c$-FA$_b$ model, indicating the smaller deterioration margin of the 40CFT-FB$_c$-FB$_b$ model. Additionally, the ductility ratio of the column base gradually deteriorated and reached a larger value in the 40CFT-FB$_c$-FB$_b$ model, compared to the 40CFT-FA$_c$-FA$_b$ model.

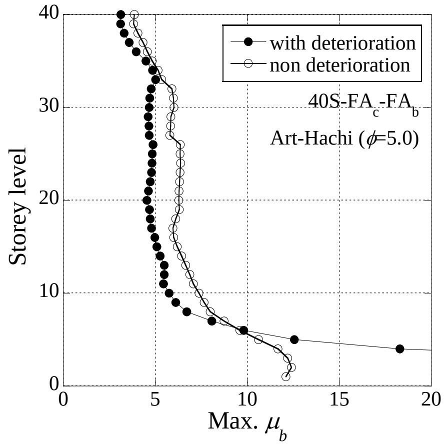

Fig. 13 Vertical beam ductility ratio distribution of 40S-FA$_c$-FA$_b$

The maximum responses of the column ductility ratio in the 40S-FA$_c$-FA$_b$ model and the beam-column components in the 40CFT-FA$_c$-FA$_b$ model did exceed 20 which is 5 times relative to the critical deformation ratio in seismic design. The failure of local components doesn't necessarily mean the overall collapse of structural systems. Moreover, the ductility of components depends on the width-thickness ratios according to various design standards for steel structures. It can be known that the sectional compactness can be divided into five levels (including S1~S5) from Chinese code, four ranks (including FA~FD) from AIJ, four categories specified in EN-1993, and middle and high ductility components in ANSI/AISC360-10. In this paper, the components in 40S-FA$_c$-FA$_b$ and 40CFT-FA$_c$-FA$_b$ were designed by using the compact FA-ranking sections as specified in AIJ.

Assuming that the section conforms to the plane section assumption, then the sectional curvature subjected to bending moment can be calculated as follows:

$$\varphi = \frac{2\varepsilon_s}{h} \tag{4}$$

where ε_s is the maximum steel strain of section, h is the height of cross-sections. The rotational angle can be obtained by integrating the curvature along the length of plastic hinge L_P which can be taken as 0.5h generally. So, the rotational angle can be expressed by:

$$\theta=\int_0^{L_p}\varphi\cdot dl=\varphi\cdot L_\mathrm{p}=\frac{2\varepsilon_s}{h}\cdot 0.5h=\varepsilon_s \tag{5}$$

For the mild steel SM490 used in this paper, the nominal yield strength σ_y is 325 MPa, the ultimate strength σ_u is 490 MPa, and Young's modulus E_s is 2.05×10^5MPa. Then when the steel reaches critical yield, the rotational angle is:

$$\theta_y=\varepsilon_y=\frac{\sigma_y}{E_s}=0.00159 \tag{6}$$

According to EN-1998, the plastic rotation capacity of the plastic hinge position shall not be less than 0.035 rad for structures with high ductility. The interlayer displacement angle can reach 0.04 rad for special steel moment-resisting frames according to ANSI/AISC341-05. Hence, when the ductility factor of members equals 20, $\theta_p = 20\theta_y = 0.0318$ which is still less than the specified plastic rotation capacity as mentioned above.

3.4 Collapse modes

The columns and beams with compact and non-compact sections in 40SMRF models and 40CFT-MRF models have the same design strength and deformation capacity according to design code, so they are comparable.

Conventionally, the plastic hinges at the collapse criterion of frames are considered by the occurrence of plastic hinges, based on the elastic-perfectly plastic assumption. While in this study, we think that the local buckling of steel members is the criteria of members' failure, and the collapse of frames is subsequently considered to be occurred by extensive local-failure of members at critical regions (e.g., the beam ends and column bases). Thus, member deterioration based on the ductility ratios of beam ends and column bases in the weak-beam frames is expected to indicate the collapse mechanism of corresponding high-rise buildings. The collapse damage of the 40S-FA$_\mathrm{c}$-FA$_\mathrm{b}$ model without and with incorporating the SD effect under the Art-Hachi wave is shown in Figures 14 (a) and 14 (b), respectively. Figures 15 (a) and 15 (b) show the collapse damage of the 40S-FB$_\mathrm{c}$-FB$_\mathrm{b}$

model without and with incorporating the SD effect under the Art-Hachi wave, respectively.

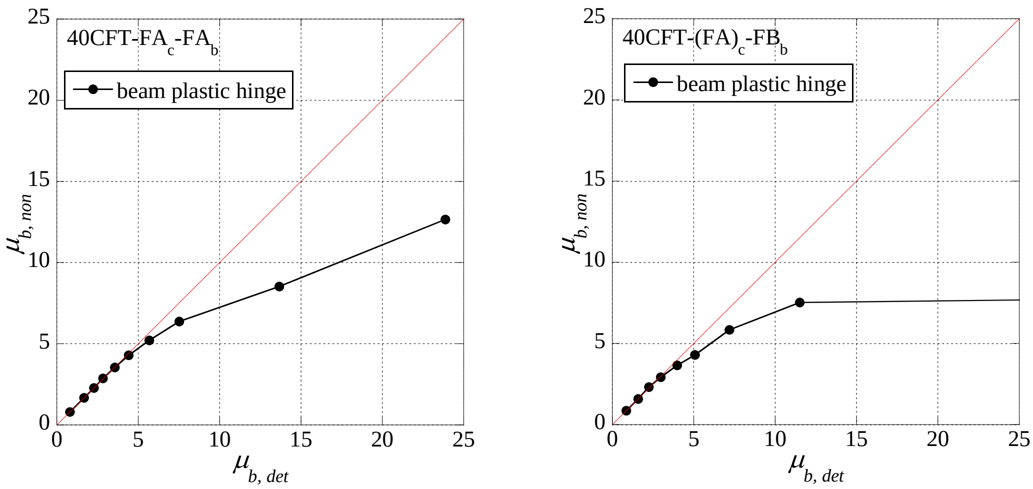

(a) 40CFT-FA$_c$-FA$_b$ model (b) 40CFT-FB$_c$-FB$_b$ model

Fig. 14 Effect of member deterioration on the beam ductility

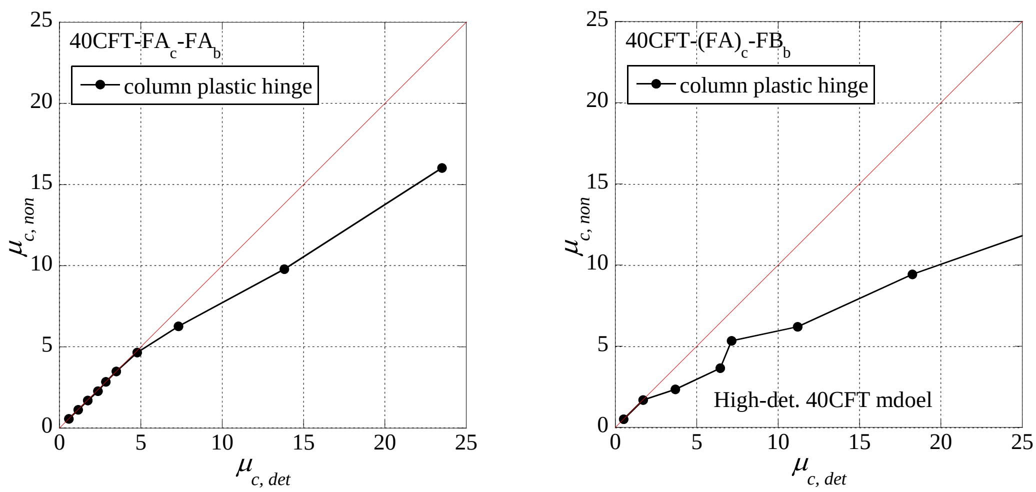

(a) 40CFT-FA$_c$-FA$_b$ model (b) 40CFT-FB$_c$-FB$_b$ model

Fig. 15 Effect of member deterioration on the column ductility

To demonstrate the distribution of plastic damages at column bases and beam ends, the ductility ratios can be divided into four levels, that is $1<\mu<2$ denoting Level 1 damage; $2<\mu<4$ denoting Level 2 damage; $4<\mu<7$ denoting median damage and $7<\mu$ denoting severe collapse-level damage.

As shown in Figure 14 (a), for the 40S-FA$_c$-FA$_b$ model, only incorporating P-Δ effect (i.e., without considering the member deterioration) resulted in the nonuniform-distribution of plastic hinges, which is similar to the bending deformation of high-rise steel building. However, as shown in Figure 14 (b) the effect of member deterioration amplified the damage extent of the 40S-FA$_c$-FA$_b$ model, resulting in larger ductility ratios of members in the lower stories, the story collapse mechanism was formed at the lower six floors. This indicates that the 40S-FA_c-FA_b model shows the ductile behavior to resist collapse being occurred. Extensively severe damages are both observed in deteriorating and non-deteriorating models at the incremental factor φ=5.0 of Art-Hachi.

By comparing Figures 15 (a) and 15 (b), for the 40S-FB_c-FB_b model, the SD effect aggravated the ductility ratios of column bases and beam ends. Additionally, all columns in the lower story failed and only some beam failed at the incremental factor φ=2.0 of Art-Hachi. These observations indicate that the 40S-FB_c-FB_b model with the non-compact section induced premature local collapse mechanism of column bases and demonstrated non-ductile behavior to resist collapse being occurred. In particular, extremely large ductility ratios of the square HST columns (μ_c) caused by column deterioration is the key reason to make the building structure collapse at the bottom story. This is consistent with the collapse phenomenon in the shaking table test of an 18-story steel frame designed by strong column weak beam criterion [Suita *et al.*, 2017]. The collapse mechanism of the beam end in lower stories and column bases in the first story occurred under the very rare earthquake with a long duration and long period. Since the damages at the beam-end change the moment distribution of column which will increase the slenderness ratio of columns, resulting in the local buckling of column base in the first story and the collapse of the lower part of the structure.

Figure 16 shows the vertical distribution of maximum ductility ratios of the beam ends in the 40S-FA_c-FA_b model with ductile collapse mode under the Art-Hachi wave. As shown in Figure 16, a relatively large ductility ratio of beams ($\mu_b \leq 15$) can still not generate collapse, but sudden increasing ductility ratios at the lower story of high-rise buildings make it collapse.

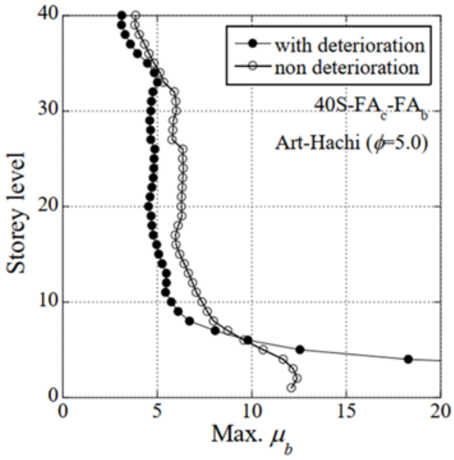

Fig. 16 Influence of strength deterioration on maximum component deformations

4 Cumulative plastic damages

4.1 Cumulative plastic deformation ratio

In addition to ductility ratio (μ), the cumulative plastic deformation ratio (η) is capable of representing the cumulative damages in terms of the hysteretic energy dissipation of the beam and column components in various high-rise building structures. Kato and Akiyama [1975] have proposed a hypothesis in which the term cumulative plastic deformation was introduced. The cumulative hysteretic energy absorbed by beam and column components during earthquake divided by the elastic limit energy of the corresponding member is defined as the component's cumulative plastic deformation ratio for beams (η_b) and columns (η_c), expressed by the following equations:

$$\begin{cases} \eta_{\mathrm{b}} = \dfrac{E_{\mathrm{h}}}{{}_{\mathrm{b}}M_{\mathrm{p}} \cdot {}_{\mathrm{b}}\theta_{\mathrm{y}}} \\ \eta_{\mathrm{c}} = \dfrac{E_{\mathrm{h}}}{{}_{\mathrm{c}}M_{\mathrm{p}} \cdot {}_{\mathrm{c}}\theta_{\mathrm{y}}} \end{cases} \tag{7}$$

where E_h is cumulative hysteretic energy dissipation at beam and column ends, which is calculated by

$$E_{\mathrm{h}} = \sum_i E_i \tag{8}$$

where ${}_bM_p$ and ${}_cM_p$ are the full-plastic flexural capacities of beam and column elements, respectively; ${}_b\theta_y$ and ${}_c\theta_y$ indicates the associated elastic rotation angles. The calculation diagrams of the ultimate energy-dissipating capacity ($M_p \cdot \theta_y$) and hysteretic energy of each cycle (E_i) are demonstrated in Figures 17 (a) and 17 (b), respectively.

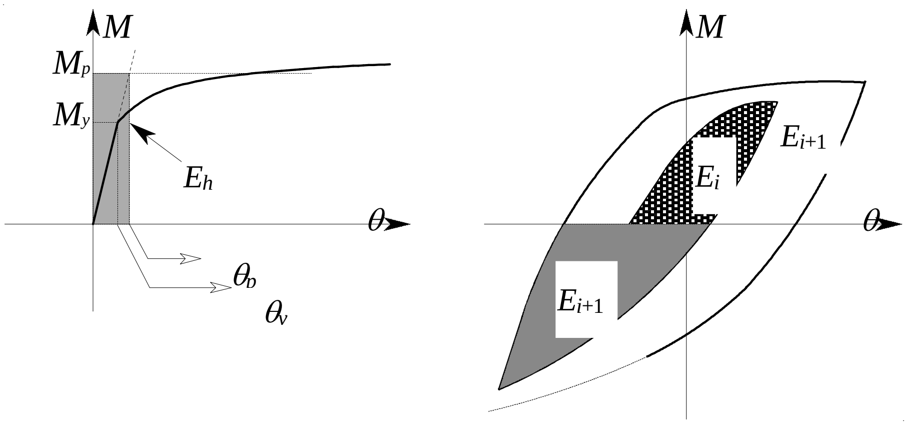

(a) Definition of $M_p \cdot \theta_p$ (b) Definition of E_h

Fig. 17 Definition of cumulative plastic deformation ratio

Likewise, the effect of member deterioration on the cumulative plastic deformation ratio of members (η_c, η_b) in the 40CFT-FA$_c$-FA$_b$ and 40CFT-FB$_c$-FB$_b$ models is also estimated. To quantify the hysteretic energy dissipated inside building structures, the (η_c, η_b) of high-rise CFT-MRFs are calculated as follows

$$\eta_{\mathrm{b,c}} = \frac{E_{\mathrm{h,max}}(\tau)}{E_{\mathrm{e}}} = \begin{cases} \dfrac{E_{\mathrm{h,max}}(\tau)}{{}_{\mathrm{b}}M_{\mathrm{p}} \times {}_{\mathrm{b}}\theta_{\mathrm{y}}}, & \text{beam} \\ \dfrac{E_{\mathrm{h,max}}(\tau)}{M_{\mathrm{u}} \times {}_{\mathrm{c}}\theta_{\mathrm{y}}}, & \text{column} \end{cases} \tag{9}$$

where the method to calculate the full-plastic moment (${}_bM_p$) of steel beams in CFT-MRFs is identical to that of H-shaped steel beams in high-rise HST building. Nonetheless, the ultimate moment (M_u) of square CFT columns [Architectural Institute of Japan, 2008], is calculated by the sum of the ultimate moment of the infill concrete (${}_cM_u$) and square steel tubes (${}_sM_u$) parts as

$$M_{\mathrm{u}} = {}_{\mathrm{s}}M_{\mathrm{u}} + {}_{\mathrm{c}}M_{\mathrm{u}} \tag{10}$$

where ${}_sM_u$ and ${}_cM_u$ can be respectively determined as follows:

$$\begin{cases} {}_{\mathrm{s}}M_{\mathrm{u}} = (1-\dfrac{t}{B})B^2 \cdot t \cdot {}_{\mathrm{s}}\sigma_{\mathrm{y}} + 2(1-x_{n1})x_{n1} \cdot {}_{\mathrm{c}}B^2 \cdot t \cdot {}_{\mathrm{s}}\sigma_{\mathrm{y}} \\ {}_{\mathrm{c}}M_{\mathrm{u}} = \dfrac{1}{2}(1-x_{n1})x_{n1} \cdot {}_{\mathrm{c}}B^3 \cdot {}_{\mathrm{c}}r_{\mathrm{u}} \cdot F_{\mathrm{c}} \end{cases} \tag{11}$$

The distribution of ultimate E_{e} of square HST and CFT columns with various ranks (FA, FB) along the structural height is presented in Figures 18 (a) and 18 (b), respectively. As shown in Figure 18, although the ultimate E_{e} of various ranks (FA, FB) of HST and CFT components is slightly different, the effect of member deterioration after peak-point show considerable influence on the collapse-resistant capacity of such high-rise buildings is still not clear. Therefore, to quantify the effect of member deterioration on the energy dissipating capacity of high-rise SMRF and CFT-MRF buildings (including Low-det. and High-det.) under over-design excitation, the time history responses of the cumulative hysteretic energy of each building model (including 40S-FA$_{\mathrm{c}}$-FA$_{\mathrm{b}}$ model, 40S-FB$_{\mathrm{c}}$-FB$_{\mathrm{b}}$ model, 40CFT-FA$_{\mathrm{c}}$-FA$_{\mathrm{b}}$ model, and 40CFT-FB$_{\mathrm{c}}$-FB$_{\mathrm{b}}$ model) where the largest cumulative plastic deformation ratio has been achieved are calculated and presented in Figures 19 and 20.

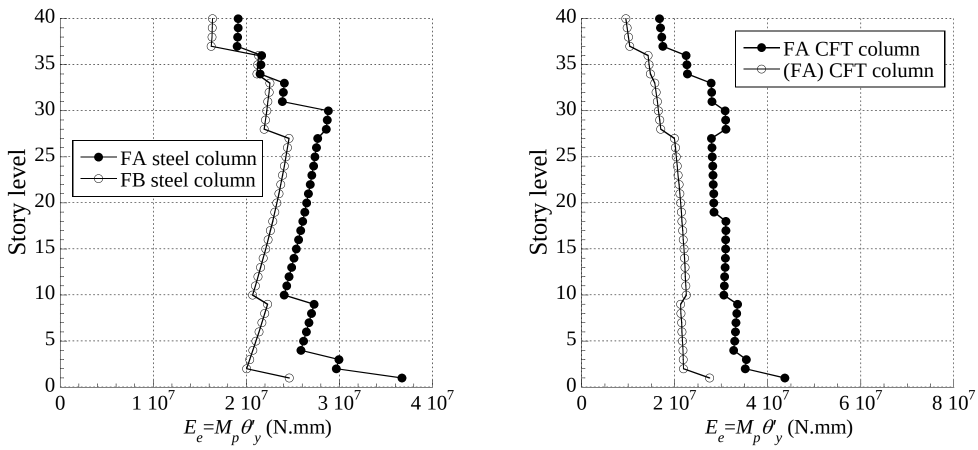

(a) HSS column (b) CFT column

Fig. 18 Energy-dissipating capacities

As shown in Figures 19 (a) and 19 (b), it can be seen that the cumulative hysteretic energy of 40S-FA$_{\mathrm{c}}$-FA$_{\mathrm{b}}$ model is larger than that of the 40S-FB$_{\mathrm{c}}$-FB$_{\mathrm{b}}$ model when the cumulative plastic deformation ratio is equal, indicating that the ultimate energy-dissipating capacity ($M_{\mathrm{p}} \cdot \theta_y$) of the 40S-FA$_{\mathrm{c}}$-FA$_{\mathrm{b}}$ model is larger than that of the 40S-FB$_{\mathrm{c}}$-FB$_{\mathrm{b}}$ model. Additionally, the 40S-FB$_{\mathrm{c}}$-FB$_{\mathrm{b}}$

model deteriorated much earlier than the 40S-FA$_c$-FA$_b$ model. Moreover, the cumulative hysteretic energy of the 40S-FB$_c$-FB$_b$ model increases rapidly and the non-ductile collapse is captured at the time of 68.4 sec of the Art-Hachi wave (φ=2.0), while the cumulative hysteretic energy of 40S-FA$_c$-FA$_b$ model gradually increased and the ductile collapse is captured at φ=5.0 of Art-Hachi wave. These phenomena indicate that the larger SD effect of non-compact steel columns reduces the collapse capacity than that of compact steel columns in the SMRF model.

As shown in Figures 20 (a) and 20 (b), for high-rise CFT moment resisting frames, it should be noted that the collapse was not captured at the end of test any matter for the 40CFT-FA$_c$-FA$_b$ model or 40CFT-FB$_c$-FB$_b$ model, indicating a higher collapse margin of high-rise CFT-MRFs, compared with SMRFs.

Differences in mechanical performance between high-rise SMRFs and high-rise CFT-MRFs can be known to form the above observations. On one hand, an extremely large cumulative plastic deformation ratio has been achieved in both the 40S-FA$_c$-FA$_b$ model and the 40CFT-FA$_c$-FA$_b$ model under severe earthquake (e.g., Art-Hachi, φ=5.0). On the other hand, for the 40S-FB$_c$-FB$_b$ model and 40CFT-FB$_c$-FB$_b$ model with high-level SD effects, as shown in Figures 19(b) and 20 (b), ignoring the member deterioration is expected to overestimate the energy dissipating capacity of the steel model, compared with the CFT-MRF model.

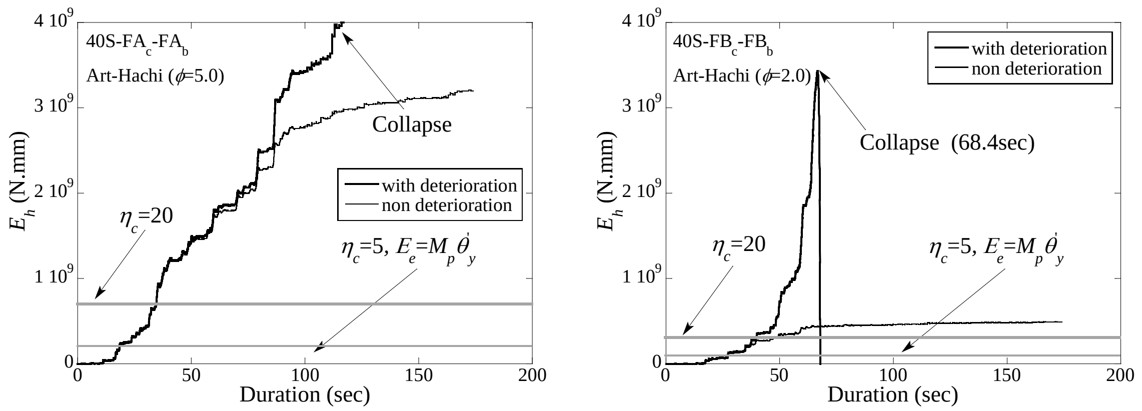

(a) 40S-FA$_c$-FA$_b$ model (b) 40S-FB$_c$-FB$_b$ model

Fig. 19 Cumulative hysteretic energy at the largest energy-dissipated element of 40SMRFs

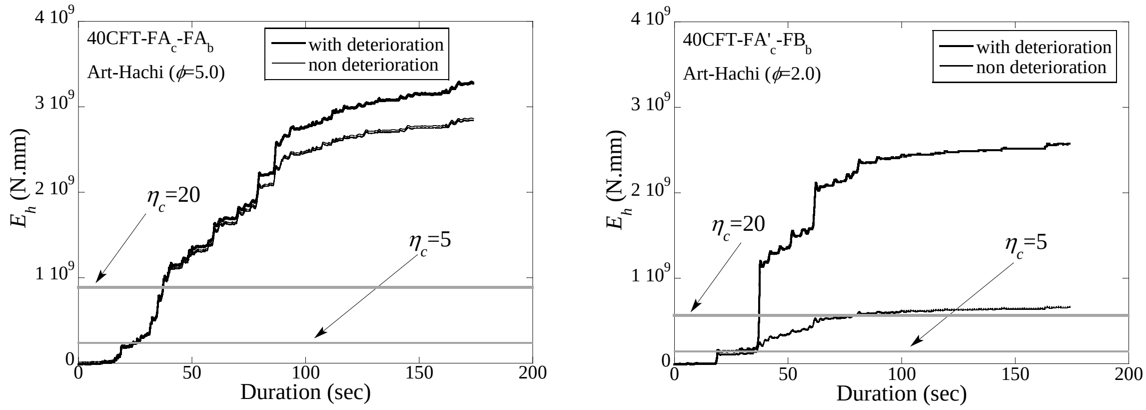

(a) 40CFT-FA$_c$-FA$_b$ model (b) 40CFT-S$_c$-FB$_b$ model

Fig. 20 Cumulative hysteretic energy at the largest energy-dissipated element of 40CFT-MRFs

4.2 Cumulative plastic deformation ratios of local members in high-rise SMRF-FB$_c$-FB$_b$ model

To quantify the cumulative energy dissipations for the incremental amplitudes of various earthquakes, the maximum cumulative plastic deformation ratio of beams (max. η_b) and columns (max. η_c) in 40S-FB$_c$-FB$_b$ models are also analyzed, as shown in Figures 21(a) and 21 (b), respectively.

It can be seen from Figure 21 that various earthquake waves induced similar incremental responses of the maximum cumulative plastic deformation ratio of beam and column, but the aleatory uncertainty caused by earthquakes is still not avoided due to the various energy inputting of each wave.

As shown in Figure 21(a), the energy-dissipating capacity of beam members deteriorates stably, while in the case of BCJ-L2 waves, the strengthening of the energy-dissipating capacity of beam is even observed, which is owing to the extreme softening (collapse) of the column. In contrast, as shown in Figure 21(b), the maximum cumulative plastic deformation ratio of column (max. η_c) is suddenly increased from initial deterioration to final collapse, which is significantly different from that of beams. This process is corresponding to the non-ductile failure of the 40S-FB$_c$-FB$_b$ model at the incremental factor φ=2.0 and shows that the collapse is mainly caused by local buckling of column bases.

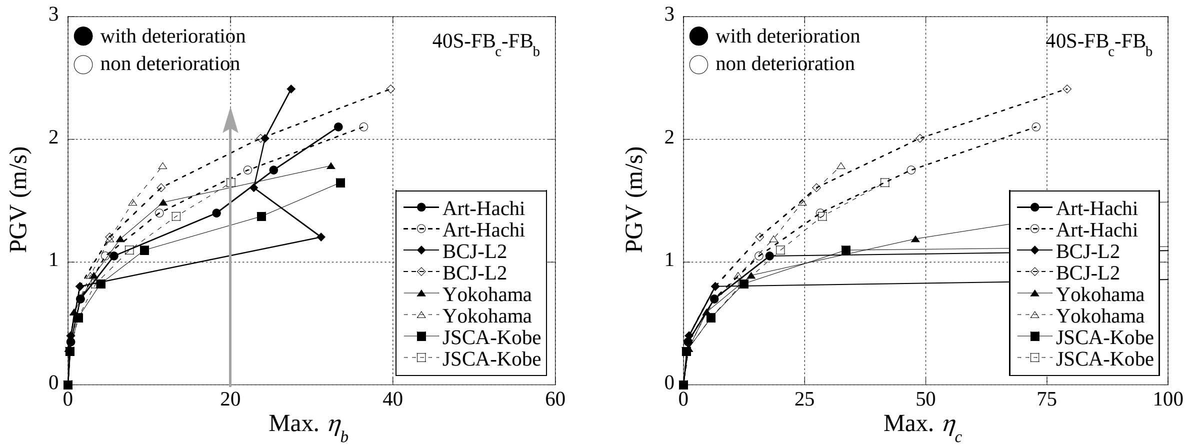

(a) Max. η_b of beam component (b) Max. η_c of column component

Fig. 21 Incremental responses of maximum cumulative plastic deflection of beams and columns

5 Conclusions

Based on the above works addressed on component plastic deformation and energy dissipation in high-rise SMRFs and CFT-MRFs considering various SD levels, the effects of SD on their deterioration and collapse mechanisms under over-design earthquake were quantified and discussed above using finite element analysis. Conclusive observations can be summarized as follows:

- Deterioration margin and collapse margin for a high-rise SMRF and CFT-MRF buildings considering various SD levels in terms of earthquake intensity PGV is given, which can be used to predict the seismic responses of high-rise SMRFs and CFT-MRFs with the long natural period under over-design earthquake directly. Even though the high-rise CFT buildings have identical horizontal stiffness with that of high-rise steel buildings, the collapse margin of high-rise CFT building is larger than that of the corresponding steel building since the composite effects of the infill concrete and the hollow steel sectional column.
- The SD effect is initiated at the lower-story portion of high-rise steel and CFT building and extended upward. The plastic hinge rotations produced at beam ends and column bases are significantly amplified by member deterioration, and the occurring of various collapse mechanisms (ductile and non-ductile) of high-rise steel buildings with deterioration can be captured.

- Deterioration margin and collapse margin based on ductility and energy for high-rise steel moment-resisting frames are completely different, but the unified processes of the deterioration and collapse producing of the beam and column members are analogical between ductility and energy.

Funding

The research described in this paper was supported by the research fellowship of Alexander von Humbolt Stiftung/Foundation [1196752] and the National Natural Science Foundation of China [51708037 and 51978076].

References

Akiyama, H. [1985] *Earthquake Resistant Limit-State Design for Buildings*, University of Tokyo Press, Tokyo.

Architectural Institute of Japan [2007] *Structural Response and Performance for Long-Period Ground Motions*, Architectural Institute of Japan, Tokyo.

Architectural Institute of Japan [2008] *Recommendations for Design and Construction of Concrete Filled Steel Tubular Structures*, Architectural Institute of Japan, Tokyo.

Bai, Y. T., Hu, H. S., Wang, J. T. and Sun, Q. [2017] "Modeling on collapse behaviour of high-rise concrete-filled steel composite frames under over-design seismic excitations," *Structure and Infrastructure Engineering* **13**(12), 1563-1575.

Bai, Y. T., Kawano, A., Odawara, K. and Matsuo, S. [2012] "Constitutive Models for Hollow Steel Tubes and Concrete Filled Steel Tubes Considering the Strength Deterioration," *Journal of Structural and Construction Engineering (Transactions of AIJ)* **77**(677), 1141-1150.

Bai, Y. T, Shi, Y. D and Deng, K. L. [2016] "Collapse analysis of high-rise steel moment frames incorporating deterioration effects of column axial force-bending moment interaction," *Engineering Structures* **127**(15),402-415.

Bojorquez, E., Reyes-Salazar, A., Teran, A. and Ruiz, S. [2010] "Energy-based damage index for steel structures," *Steel and Composite Structure* **10**(4).

Diaz, S. A., Pujades, L. G., Barbat, A. H., Vargas, Y. F. and Hidalgo-Leiva, D. A. [2017] "Energy damage index based on capacity and response spectra," *Engineering Structures* **152**, 424-436.

Fajfar, P. and Gaspersic, P. [1996] "The N2 Method for the Seismic Damage Analysis of RC Buildings," *Earthquake Engineering and Structural Dynamics* **25**(1), 31-46.

Housner, G. W. [1956] "Limit design of structures to resist earthquakes," *Proc. of the First World Conference on Earthquake Engineering*, Vol. 5, San Francisco, pp. 1–13.

Heidari, A. and Gharehbaghi, S. [2015] "Seismic performance improvement of Special Truss Moment Frames using damage and energy concepts," *Earthquake Engineering and Structural Dynamics* **44**(7), 1055-107.

Karavasilis, T. L., Kerawala, S. and Hale, E. [2012] "Hysteretic model for steel energy dissipation devices and evaluation of a minimal-damage seismic design approach for steel buildings," *Journal of Constructional Steel Research* **70**, 358-367.

Ke, K., Yam, M. C.H. and Ke, S. [2017] "A dual-energy-demand-indices-based evaluation procedure of damage-control frame structures with energy dissipation fuses," *Soil Dynamics and Earthquake Engineering* **95**, 61-82.

Khashaee, P. [2005] "Damage-based Seismic Design of Structures," *Earthquake Spectra* **21**(2), 371-387.

Lin, X., Kato, M., Zhang, L. and Nakashima, M. [2018] "Quantitative investigation on collapse margin of steel high-rise buildings subjected to extremely severe earthquakes," *Earthquake Engineering and Engineering Vibration* **17**(3), 445-457.

Manegotto, M. and Pinto, PE [1973] "Method of Analysis for Cyclically Loaded RC Plane Frames Including Changes in Geometry and Non-elastic Behaviour of Elements under Combined Normal Force and Bending," *IABSE Symposium on Resistance and Ultimate Deformability of Structures Acted on by Well-Defined Repeated Loads*, Lisbon, Portugal, pp. 15–22.

Mehanny, S. S. F. and Deierlein, G. G. [2001] "Seismic Damage and Collapse Assessment of

Composite Moment Frames," *Journal of Structural Engineering* **127**(9), 1045-1053.

Suita K., Suzuki Y. and Takahashi S. [2017] "Collapse behavior study of 18-story steel structure building based on shaking table test," *Building Structure* **47**(16), 1-8.

Spacone, E. and El-Tawil, S. [2004] "Nonlinear Analysis of Steel-Concrete Composite Structures: State of the Art," *Journal of Structural Engineering* **130**(2), 159-168.

Uetani, K. and Tagawa, H. [1996] "Deformation Concentration Phenomena in the Process of Dynamic Collapse of Weak-Beam-Type Frames," *Journal of Structural and Construction Engineering (Transactions of AIJ)* **483**(5), 51-60.

Vamvatsikos, D. and Cornell, C. A. [2002] "Incremental Dynamic Analysis," *Earthquake Engineering and Structural Dynamics* **31**, 491-514.

Wakabayashi, M. [1986] *Design of Earthquake-Resistant Buildings* McGraw-Hill, Inc., New York.

Wong, K. K. F. and Harris, J. L. [2012] "Seismic damage and fragility analysis of structures with tuned mass dampers based on plastic energy," *The Structural Design of Tall and Special Buildings* **21**(4), 296-310.

Table 1 Slenderness ranks of column and beam

Section	Member	Geometry	Width-to-thickness ratio	
			FA	FB

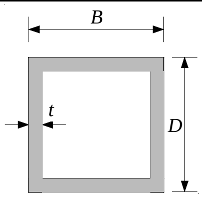	Column	*B/t*	$<33\sqrt{235/F}$ (28.1 for F=325 MPa)	$33\sqrt{235/F}$ <*B/t*< $37\sqrt{235/F}$ (31.5 for F=325 MPa)
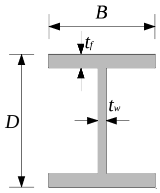	Beam	Flange (B/t_f)	$9\sqrt{235/F}$ (7.65for F=325 MPa)	$11\sqrt{235/F}$ (9.35 for F=325 MPa)
		Web (D/t_w)	$60\sqrt{235/F}$ (51 for F=325 MPa)	$65\sqrt{235/F}$ (55.25 for F=325 MPa)

Note: *F* is yield strength of steel materials.

Table 2 Characteristic points about strength deterioration

Section	Member	Criteria of Width-thickness ratio (*B/t*)	
		FA	FB

	Column	$<33\sqrt{235/F}$ (28.1 for F=325 MPa)	$33\sqrt{235/F}$ $<B/t<$ $37\sqrt{235/F}$ (31.5 for F=325 MPa)
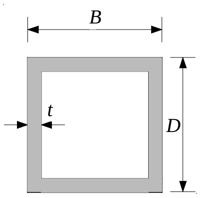	τ_{lb}	<0.04	<0.06
	ε_{lb}	>0.0086	>0.0064
	$\varepsilon_{lb}/\varepsilon_y$	>4.31	>3.18
	γ	>0.69	>0.65

Note: τ_{lb} is the ratio of negative modulus compared to Young's modulus; ε_{lb} the critical strain corresponding to stress deterioration; ε_y is the yield strain; γ is the residual stress after strength deterioration.

Table 3 Cross sections of members in 40S-FA$_c$-FA$_b$ model

Story level	Exterior column	Interior column	Beam

	Sectional parameter $B \times t$ (mm)	B/t	Sectional parameter $B \times t$ (mm)	B/t	Sectional parameter $D \times B \times t_w \times t_f$ (mm)
1~3	□700×45	15.6	□750×50	15.0	850×400×19×36
4~6			□750×45	16.7	
7~9	□700×40	17.5	□700×50	14.0	
10~12			□700×45	15.6	
13~18	□700×36	19.4	□650×50	13.0	
19~27			□650×45	14.4	
28~30	□650×40	16.3	□650×40	16.3	800×400×19×36
31~33	□600×36	16.7	□600×40	15.0	800×350×19×36
34~36	□600×32	18.8	□600×32	18.8	800×350×16×28
37~40	□600×28	21.4	□600×28	21.4	750×300×16×28

Table 4 Cross sections of members in 40S-FB_c-FB_b model

Story level	Exterior column		Interior column		Beam
	Sectional parameter $B\times t$ (mm)	B/t	Sectional parameter $B\times t$ (mm)	$B/$t	Sectional parameter $D\times B\times t_w\times t_f$ (mm)
1~3	□850×28	30.4	□950×32	29.7	1000×400×19×25
4~9			□900×32	28.1	
10~12	□800×28	28.6	□900×32	28.1	
13~27	□800×28	28.6	□850×28	30.4	
22~27			□800×28	28.6	
28~30	□800×25	32.0	□800×25	32.0	900×400×16×32
31~33			□800×25	32.0	900×350×16×32
34~36	□750×25	30.0	□750×25	30.0	800×400×14×28
37~40	□650×22	29.5	□650×22	29.5	800×300×14×28

Table 5 The natural periods of SMRFs and equivalent CFT-MRFs models

S-MRF model	Analogous CFT model	Height	Square column	H-shaped steel beam	T_1 of CFT model	T_1 of steel model
40S-FA_c-FA_b	40CFT-FA_c-FA_b	161m	FA	FA	4.38s	4.67s
40S-FB_c-FB_b	40CFT-FB_c-FB_b	（40-story）	FB	FB	4.12s	4.53s